ORIGINAL ARTICLE

Journal Section

Quantum-rotor-induced Polarization

Benno Meier[1]*

[1]School of Chemistry, University of Southampton, United Kingdom

Correspondence
Benno Meier, School of Chemistry, University of Southampton, Southampton, Hampshire, SO17 1BJ, United Kingdom
Email: b.meier@soton.ac.uk

Funding information
EPSRC (UK) EP/N002482/1, EP/M001962/1

Quantum-rotor-induced polarization is closely related to para-hydrogen-induced polarization. In both cases the hyperpolarized spin order derives from rotational interaction, and the Pauli principle by which the symmetry of the rotational ground state dictates the symmetry of the associated nuclear spin state. In quantum-rotor-induced polarization there may be several spin states associated with the rotational ground state, and the hyperpolarization is typically generated by hetero-nuclear cross-relaxation. This review discusses preconditions for quantum-rotor-induced polarization for both the 1-dimensional methyl rotor and the asymmetric rotor $H_2^{17}O@C_{60}$, i.e. a single water molecule encapsulated in fullerene C_{60}. Experimental results are presented for both rotors.

KEYWORDS
Quantum-rotor-induced polarization, Hyperpolarization, Nuclear Spin Conversion, Spin Isomerism, Methyl, Water

1 | INTRODUCTION

Nuclear hyperpolarization is concerned with the generation of non-equilibrium spin polarization, which is typically 10 to 10 000-fold larger than its thermal equilibrium analogue. Hyperpolarization seeks to enhance the signal, and thereby the sensitivity of magnetic resonance, with a prospect of revolutionary applications in fields spanning from materials science to healthcare [1, 2, 3, 4, 5, 6].

The signal in magnetic resonance is directly proportional to the polarization of the nuclear spin states, which, for an ensemble of spins $1/2$ in thermal equilibrium, is given by the Boltzmann distribution:

$$p = \tanh\left(\frac{\hbar\gamma B}{2kT}\right) \tag{1}$$

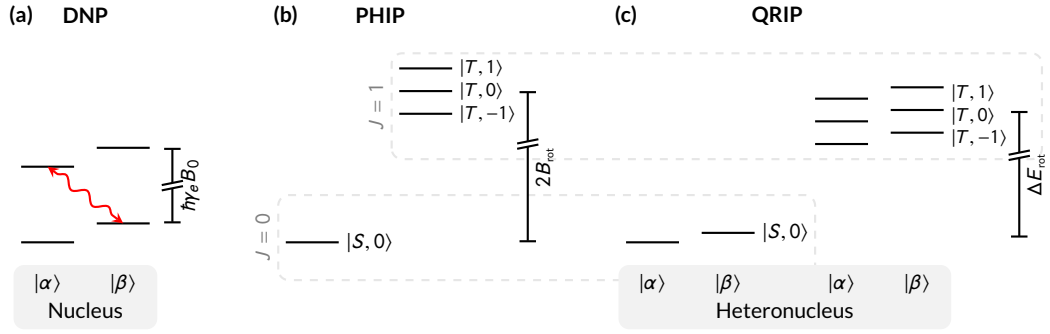

FIGURE 1 Hyperpolarization mechanisms. (a) In dynamic nuclear polarization nuclear spins states are actively coupled to electron spin-states using microwave irradiation, as indicated by the red line. $|\alpha\rangle$ and $|\beta\rangle$ designate the spin state of the nucleus. (b) In para-hydrogen induced polarization, the $J = 0$ state is associated with the nuclear singlet state, and the $J = 1$ state is associated with the nuclear triplet states, leading to a large splitting between these states. (c) In dissolution-quantum-rotor-induced polarization the situation is similar. The rotational splitting depends on the rotational Hamiltonian, and may be reduced strongly if the rotation is hindered. In addition a heteronucleus is required to release the spin order following a temperature jump.

The most basic hyperpolarization strategy is brute-force hyperpolarization, in which the spin polarization is enhanced simply by equilibrating the sample at very low temperatures. Milli-Kelvin temperatures are required to achieve near unity spin polarization, but the spin-lattice relaxation time at such low temperatures becomes prohibitively long, limiting the attainable polarization enhancement in high-field experiments to roughly 100 [7, 8].

Other hyperpolarization strategies work by coupling the nuclear spin states to other states that display a larger splitting, and hence a larger polarization at a given temperature. The cases of dynamic nuclear polarization (DNP), para-hydrogen induced polarization (PHIP) and quantum-rotor-induced polarization (QRIP) are illustrated in Fig. 1.

In DNP [9, 10, 11], cf. Fig. 1a), the other states are those of a free electron spin, split by the electron Zeeman interaction, $\Delta E = -\hbar\gamma_e B_0$. At a given field the splitting between the two electron spin states is 660 times larger than that of the two proton spin states. Forbidden electron-nuclear transitions can be driven using microwave irradiation, and the proton spin polarization can be enhanced by a factor of up to 660. DNP is now routinely used in magic angle-spinning NMR [12, 13, 14, 15], with typical enhancements of the order of 100. Even larger enhancements are obtained if the DNP process is driven at a temperature much lower than the temperature at which the polarization is measured. In dissolution-dynamic nuclear polarization (D-DNP) [16, 17, 18, 19] the DNP process is driven at a field of typically 7 Tesla and a temperature of approximately 1 Kelvin. Under these conditions the electron spins are fully polarized, and it is possible to establish a nuclear spin polarization of several 10 percents. In favorable cases a rapid dissolution of the polarized sample essentially preserves the nuclear spin polarization. The corresponding signal enhancements, due to both DNP and the temperature jump during dissolution, of 10 000 and more have enabled in particular the tracking of human metabolic fluxes *in vivo* [2].

In PHIP [20, 21], cf. Fig 1b), the larger splitting is that of the rotational states of the dihydrogen molecule, $\Delta E = 2B_{\mathrm{rot}}$, where B_{rot} is the rotational constant of dihydrogen. The nuclear spin order arises as a consequence of the Pauli principle: The wavefunction must be antisymmetric under exchange of the two protons. The overall wavefunction is simply the product of the rotational part and the nuclear spin part. Therefore, the symmetric $J = 0$ rotational ground state is associated with the anti-symmetric singlet state $|S,0\rangle$ and belongs to the set of *para*-states. The antisymmetric $J = 1$ rotational state is associated with the $|T,i\rangle, i \in \{-1,0,+1\}$ triplet states that designate *ortho*-hydrogen. Note that the

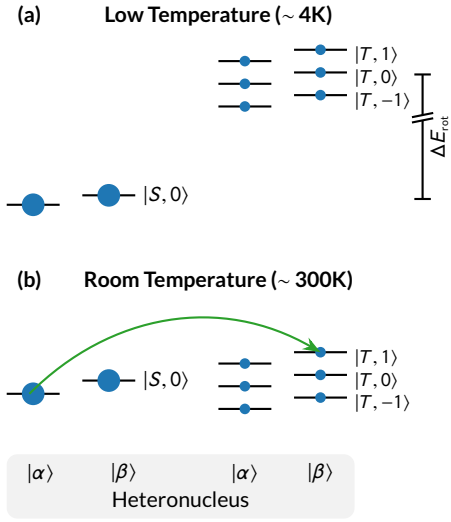

FIGURE 2 Quantum-rotor-induced polarization. (a) Symmetry order is created by equilibrating a substance with a substantial rotational splitting at low temperature. (b) Upon dissolution higher rotational states are populated, leading to an average Hamiltonian with a substantially reduced rotational splitting. Initially the net population difference across observable transitions is zero, but cross-relaxation processes such as the indicated zero quantum transition (green line) convert the symmetry order into observable Zeeman polarization.

spin quantum number describing the spin projection onto the applied field is often written as a subscript, i.e. $|T_i\rangle$. Here I have chosen a different notation for consistency with the spin states of the methyl rotor.

The nuclear spin states are

$$|S,0\rangle = (|\alpha\beta\rangle - |\beta\alpha\rangle)/\sqrt{2} \tag{2}$$

$$|T,-1\rangle = |\alpha\alpha\rangle$$

$$|T,0\rangle = (|\alpha\beta\rangle + |\beta\alpha\rangle)/\sqrt{2} \tag{3}$$

$$|T,1\rangle = |\beta\beta\rangle$$

The splitting between the two lowest rotational states of dihydrogen is $2B \sim 175$ Kelvin, and nearly pure para-hydrogen is obtained by flowing hydrogen gas over a catalyst at a temperature of 20 Kelvin, just above the boiling point of dihydrogen. The catalyst is required as the equilibration of dihydrogen requires a simultaneous change in the symmetry of the rotational part (as it changes from $J = 1$ to $J = 0$) and the spin part (changing from $|T,i\rangle$ to $|S,0\rangle$). If, after equilibration at low temperature, the hydrogen gas is warmed up to room temperature in the absence of catalytic elements, the *ortho/para* ratio established at low temperatures is preserved. Such order is also referred to in the literature as singlet order [22], triplet-singlet imbalance [23] or symmetry order [24].

In conventional PHIP, the spin order is released via hydrogenation of the target molecule with para-hydrogen. The transfer of spin hyperpolarization from para-hydrogen to a substrate can also occur if para-hydrogen is bound only reversibly to a metal center. So called Signal Amplification by Reversible Exchange (SABRE), invented by Duckett and co-workers [3], has substantially broadened the scope of para-hydrogen induced polarization [21].

In QRIP (Fig. 1c), the large splitting ΔE_{rot} is also that of the rotational state of either the entire molecule, or a

rotating moiety, such as a methyl group. This splitting depends on the rotational Hamiltonian, and decreases rapidly if the rotation is hindered. Both PHIP and QRIP therefore exploit a rotational Hamiltonian to generate symmetry order. In this sense QRIP is a generalization that extends the concept of PHIP to quantum rotors other than dihydrogen. PHIP is then a manifestation of QRIP, and other manifestations of QRIP are the Haupt effect, in which hyperpolarized signals are observed in the solid state, and an effect that would more specifically be termed D-QRIP, in which hyperpolarized signals are observed in solution following a temperature jump, in analogy to D-DNP. In the literature the term QRIP refers exclusively to such D-QRIP effects. For the remainder of this manuscript I will use the more specific term D-QRIP when appropriate. In D-QRIP the symmetry order is released by cross-relaxation following a temperature jump, with the dominating relaxation mechanism being heteronuclear dipole-dipole relaxation.

The most basic quantum rotor that could display this effect is perhaps hydrogen selenide $H_2^{77}Se$, comprising only two equivalent protons and one spin-1/2 heteronucleus. This system serves here only to illustrate the concept. An observation of quantum-rotor-induced polarization on $H_2^{77}Se$ will only be possible if a way is found to preserve free rotation of the molecule at low temperatures. The lowest energy levels for this molecule are shown in Fig. (1c). As can be seen, the energy level structure for this molecule is completely analogous to that of dihydrogen, but the introduction of the spin-1/2 ^{77}Se heteronucleus introduces a further quantum number. The additional spin does not lead to a significant change of the rotational energy structure, and para-H_2Se is enriched by equilibrating the material at low temperatures as depicted in Fig. 2a). Upon dissolution higher rotational states become accessible. Rapid transitions occur only between states of the same symmetry, but lead to a greatly reduced average splitting [25], as depicted in Fig. 2b). Now heteronuclear cross-relaxation processes unevenly populate observable transitions, thereby leading to the antiphase spectra characteristic for D-QRIP.

Historically, the first observation of D-QRIP was reported by Maik Icker and Stefan Berger in 2012 [26, 27] on the ^{13}C-methyl moiety of γ-picoline. In 2013, the Levitt group published a paper that confirmed the observations of the Berger group but furthermore presented a study of how the polarization of the $^{13}CH_3$ spin system evolved in time. Due to the close analogy with long-lived states, a slow decay was anticipated, and indeed the symmetry order decayed approximately 7 times more slowly than T_1, constituting the first experimental evidence for long-lived states in methyl groups [28]. A more thorough description of the theory of long-lived spin states in methyl groups has since been given by Dumez, Levitt and co-workers [29]. A further analysis with a focus on dipolar cross-relaxation has been given by Annabestani and Cory [24]. Symmetry order in methyl groups can also be established using dynamic nuclear polarization [30, 31].

Here, I do not reiterate the details of the relaxation mechanisms of long-lived spin order in methyl or other quantum rotors - these have been described in detail by Dumez et al. [29] - but focus on theoretical and experimental considerations for the establishment and observation of symmetry order in quantum rotors. To the best of my knowledge, methyl groups and fullerene-encapsulated, ^{17}O-labelled water are the only quantum rotors in which D-QRIP has been observed to date. I will discuss theoretical and experimental aspects for these two systems.

2 | THEORY

2.1 | Methyl - the 1D rotor

The subject of methyl rotation has been reviewed extensively by Horsewill [25]. In analogy to *ortho* - and *para*-water the nuclear spin states of the three methyl protons are classified corresponding to their symmetry as $|A\rangle$ or $|E_a\rangle$ or $|E_b\rangle$ states, where A and $E_{a,b}$ correspond to irreducible representations of the symmetry group C_3. The Pauli principle requires the product of spin and rotational state to be of symmetry A [32].

In analogy to the triplet states of *ortho*-water the $|A\rangle$ states are symmetric under spin permutation. They are

$$\begin{aligned} |A,3/2\rangle &= |\alpha\alpha\alpha\rangle \\ |A,1/2\rangle &= (|\alpha\alpha\beta\rangle + |\alpha\beta\alpha\rangle + |\beta\alpha\alpha\rangle)/\sqrt{3} \\ |A,-1/2\rangle &= (|\alpha\beta\beta\rangle + |\beta\alpha\beta\rangle + |\beta\,\beta\alpha\rangle)/\sqrt{3} \\ |A,-3/2\rangle &= |\beta\beta\beta\rangle \end{aligned} \tag{4}$$

The E_a states have total spin $1/2$:

$$\begin{aligned} |E_a,1/2\rangle &= \left(|\alpha\alpha\beta\rangle + \epsilon\,|\alpha\beta\alpha\rangle + \epsilon^*\,|\beta\alpha\alpha\rangle\right)/\sqrt{3} \\ |E_a,-1/2\rangle &= \left(|\alpha\beta\beta\rangle + \epsilon\,|\beta\alpha\beta\rangle + \epsilon^*\,|\beta\,\beta\alpha\rangle\right)/\sqrt{3}, \end{aligned} \tag{5}$$

where $\epsilon = \exp(\mathrm{i}2\pi/3)$. The $|E_a\rangle$ states acquire a phase ϵ^* under cyclic permutation. The $|E_b\rangle$ states have total spin $1/2$ as well. They are obtained by the transformation $\epsilon \leftrightarrow \epsilon^*$, and acquire a phase ϵ under cyclic permutation.

In exactly the same way that para-hydrogen experiments require singlet order, or a triplet-singlet imbalance (TSI) [33], experiments involving QRIP in methyl also require symmetry order or, more specifically an imbalance between $|A\rangle$ and $|E\rangle$ states. The splitting between $|A\rangle$ and $|E\rangle$ states, referred to as *tunneling splitting*, is typically required to be of the order of a few Kelvin, so that an imbalance can be achieved by equilibrating the material in a bath of liquid helium at 4.2 Kelvin.

The decisive nature of the tunneling splitting may be difficult to appreciate [34, 35], and I therefore discuss it in greater detail here.

Consider the Hamiltonian for a methyl group that is rotating along its symmetry axis:

$$\mathcal{H} = \frac{\hat{J}^2}{2I} = -\frac{\hbar^2}{2I}\frac{\partial^2}{\partial\phi^2} + V(\phi). \tag{6}$$

The first term describes the kinetic energy, with the methyl moment of inertia given as $I = 5.3\times10^{-47}$ kg/m^2. An entirely freely rotating methyl group has $V(\phi) = 0$, and the eigenfunctions are given as

$$|m\rangle = \frac{1}{\sqrt{2\pi}}\mathrm{e}^{\mathrm{i}m\phi}, \quad m = 0, \pm1, \pm2, \ldots \tag{7}$$

The energy of the m-th state is $\hbar^2 m^2/2I$. Except for $m = 0$, the free rotor states are therefore doubly degenerate. The energy of the $m = 1$ state in particular is ~ 0.65 meV ~ 7 K.

The potential $V(\phi)$ has to respect the 3-fold symmetry of the methyl group, and in general can be written as a Fourier series [25]. While the energy structure may be altered by additional interactions such as rotor-rotor couplings [36], here I illustrate the concept using only a 3-fold potential, i.e. the first term of the Fourier series:

$$V(\phi) = \frac{V_3}{2}\left[1 - \cos(3\phi)\right] \tag{8}$$

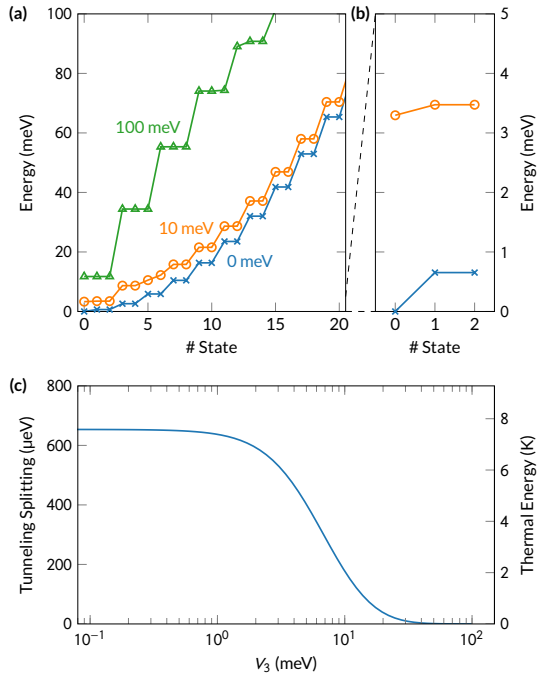

FIGURE 3 Energy structure of the hindered methyl rotor. (a) Energy of the n-th rotational state for three different strengths of the hindering barrier V_3. In the case of $V_3 = 0$ (blue, crosses) one obtains the eigenstates of the free rotor. The zoom in panel (b) clearly reveals the splitting between the two lowest rotational states. A small barrier of 10 meV (orange, open circles) reduces the splitting between the zeroth and the first rotational state. In the limit of a strong barrier of $V_3 = 100$ meV (green, filled circle) the lower rotational states are triply degenerate, with the energy structure of a harmonic oscillator. (c) Tunneling splitting as a function of the barrier strength.

The matrix elements for this interaction in the basis of Eq. 7 are

$$\langle m|\, V(\phi)\, |n\rangle = \frac{V_3}{4\pi^2}\int_0^{2\pi} \mathrm{e}^{-\mathrm{i}m\phi}[1-\cos(3\phi)]\mathrm{e}^{\mathrm{i}n\phi}\mathrm{d}\phi = \frac{V_3}{4}\left[2\delta_{mn} - \delta_{3,n-m} - \delta_{-3,n-m}\right] \tag{9}$$

A numeric diagonalization of $\mathcal{H}$ yields the energies of the rotational states. An implementation in Python is listed in the appendix. The energies are shown for three different values of V_3 in Fig. 3a). In the case of $V_3 = 0$ (blue curve, crosses) the energies are simply the energies of the free rotor. Apart from the non-degenerate ground-state, each rotational state is doubly degenerate. A small barrier of 10 meV (orange curve, open circles) mixes the lowest rotational ground-states. In the limit of a strong barrier, $V_3 = 100$ meV (green, filled circles), the lower rotational states are those of a harmonic oscillator. The states are triply degenerate in correspondence to the three-fold potential, and equally spaced at low energies.

The tunneling splitting is calculated as the difference in energy of the first and zeroth rotational state, cf. ΔE_{rot} in Fig. 1. It is shown as a function of the hindering potential V_3 in Fig. 3c). The term can be misleading in the limit of an entirely free rotor as there is no barrier and hence no tunneling - in this case the tunneling splitting is simply the splitting between the two lowest rotational states. If a barrier is introduced, the first and zeroth state remain only non-degenerate to the extent that tunneling is allowed through the rotational barrier [37]. The tunneling splitting

corresponds to only 1 Kelvin at a barrier strength of 10 meV, and quickly goes to zero as the barrier strength is increased further. The corresponding thermal energy is shown on the right-hand ordinate of Fig. 3c). It can be seen that liquid helium temperatures (approximately 1-4.2 Kelvin) can only induce population imbalances between *A* and *E* states as long as the barrier does not exceed $\sim$ 10 meV. Quantum rotation is therefore not the source of the hyperpolarized signals observed by Ludwig et al. [34] on substances which exhibit only a tiny tunneling splitting - these signals originate from a nuclear Overhauser effect as was shown elsewhere [38].

2.2 | Water - the asymmetric rotor

Water may rotate about each of its principal axes, and in analogy to Eq. 6 the Hamiltonian is written as

$$\mathcal{H} = \frac{\hat{J}_a^2}{2I_a} + \frac{\hat{J}_b^2}{2I_b} + \frac{\hat{J}_c^2}{2I_c} \tag{10}$$

To find the energies, the angular momentum operators $\hat{J}_i$ are expressed in terms of $\hat{\boldsymbol{J}}^2$, $\hat{J}_z$, and $\hat{J}_\pm$. The matrix elements are then computed in a symmetric top basis $|J, k\rangle$ with $k \in -J, \ldots J$, and the Hamiltonian is diagonalized as above. The full procedure has been described in detail by Bunker and Jensen [39]. For freely rotating water, the splitting between the lowest rotational states is approximately 30 K, and hence water can be enriched in its rotational ground state by equilibrating it at a temperature below 30 Kelvin. Any hindering potential would of course greatly reduce the rotational splitting in analogy to the 1D rotor discussed above. A water molecule encapsulated in a fullerene cage retains its freedom to rotate, and it is only for this reason that quantum-rotor-induced polarization can be observed in these systems. In full analogy to para-hydrogen the symmetric rotational ground state requires an anti-symmetric spin state, and the rotational ground state of water is therefore *para*-water, with the nuclear spin state being the singlet state given by Eq. 2. The first excited state is an *ortho*-state with the three nuclear spin states being the triplet states given by Eq. 3.

Note that the above discussion of methyl and water ignores the presence of the heteronucleus as it is not important for the rotational energy structure. It can be taken into account by forming a direct product of a given state with the spin state of the heteronucleus, e.g. $|A, 3/2\rangle \otimes |1/2\rangle$ for a methyl moiety in the given *A* state with a carbon in the $+1/2$ state.

3 | EXPERIMENTAL ASPECTS

3.1 | Solid state

The energy structure of quantum rotors enables their study by a large range of spectroscopic techniques. Neutron scattering [40, 41, 42] and infrared spectroscopy [42] can directly probe the energy structure. Magnetic resonance does not directly probe the energy structure, but temperature-jump experiments can be used to study conversion between the *A* and *E* states of methyl groups or between the *para* and *ortho* states of water. The conversion process between the different symmetry species has been termed *nuclear spin conversion*, *spin isomer conversion* or, in the case of water or dihydrogen, *ortho-para*-conversion. The first spin isomer conversion experiments have been performed by Haupt [43, 44]. He observed strongly enhanced dipolar order on the methyl protons of 4-methyl-pyridine (also refered to as γ-picoline) when changing the temperature between approximately 30 Kelvin and 10 Kelvin. It has also been shown that the hyperpolarization can be transferred to other nuclei in the solid using cross-polarization [45], and that the effect is independent of magnetic field [46].

Nuclear spin conversion of small molecules like water can only be observed if the required free rotation of the water molecules is retained. One strategy is to isolate them in solid matrices of inert gases like argon [47, 48]. However, this

approach provides little control over the environment of the dissolved molecules, and is prone to the formation of dimers or clusters. Molecular endofullerenes such as $H_2O@C_{60}$ [49, 50, 42], in which a single, freely rotating water molecule is enclosed in a fullerene cage, provide an excellent alternative. These systems are very homogeneous, and provide an approximately 2 molar concentration of water molecules, amenable for study with nuclear magnetic resonance. In solid $H_2O@C_{60}$ spin conversion at low temperatures is readily monitored by NMR [51]. Following a temperature jump from 30 to 5 Kelvin, the excess *ortho*-water converts to NMR silent *para*-water, leading to a reduction in the NMR signal. The conversion kinetics are best described using a second order model, indicating that interaction between the water molecules facilitates the conversion.

Water exhibits an electric dipole moment, and therefore a Stark effect: an applied electric field shifts the rotational energies. The electrical polarizability of a water molecule is obtained as the second derivative of its energy with respect to the applied field, and depends on the rotational state. It is therefore possible to seperate *ortho* and *para*-water using electric field gradients [52], and it is also possible to monitor the spin conversion by measuring the dielectric constant of the material [53]. This is a convenient method in practice as capacitive detection is simple and rather sensitive.

3.2 | Solid-to-liquid temperature jumps

3.2.1 | Methyl groups

Transient phenomena can be observed with liquid-state NMR if a quantum-rotor polarized sample is dissolved in warm solvent. In the first experiments of this kind, conducted by Icker and Berger [26], a small amount of 4-methyl-pyridine was loaded into an NMR tube that was subsequently kept in liquid helium for half an hour to generate quantum-rotor polarization. The material is then dissolved by adding acetone-d_6, and the NMR tube is loaded into an NMR spectrometer followed by an acquisition of the NMR signal.

The first study of the time evolution of these signals was reported by the Levitt group [28], using a dissolution apparatus as first described by Ardenkjær-Larsen and co-workers [16]. A similar apparatus has also been used in recent experiments by Dumez et al., where dynamic nuclear polarization was used as an alternative means to create symmetry order in substances bearing methyl groups [31].

In order to generate quantum-rotor polarization one only needs to equilibrate the material at low temperature - no magnetic field is required. The same argument applies to the transfer of the sample. While fast-relaxation can rapidly quench spin polarization in solid samples at low fields [8], this is not a concern for quantum-rotor polarization. The possibility of transferring a sample in the solid then allows for a much faster transfer, as one is not limited by the friction that occurs between a liquid and the walls of the tube through which the liquid is flushed. In a simple apparatus the material of interest is loaded into a teflon capsule. This “bullet” is then loaded into a U-shaped steel tube that is installed in an Oxford Instruments Flow-Cryostat. The sample is kept cold for the required time, and then ejected rapidly using pressurized helium gas. A receiver structure in the liquid-state NMR apparatus retains the capsule but allows for the sample to travel further into an NMR tube preloaded with solvent. The time required for the material to dissolve depends on the used solvents, but is typically of the order of 1 s in ambient temperatures solutions. Generally it is desirable to dissolve the material quickly to reduce additional losses that may occur as the sample melts. In addition to minimizing sample dilution, a key advantage is that the sample is transferred very quickly (approximately 100 ms), and therefore one can also monitor the buildup of magnetization immediately after dissolution, without having to revert to procedures such as a T_{00} filter that substantially perturb the spin system. Experimental results obtained with this apparatus are shown in Fig. 4. A more detailed description of this apparatus has been given elsewhere [54].

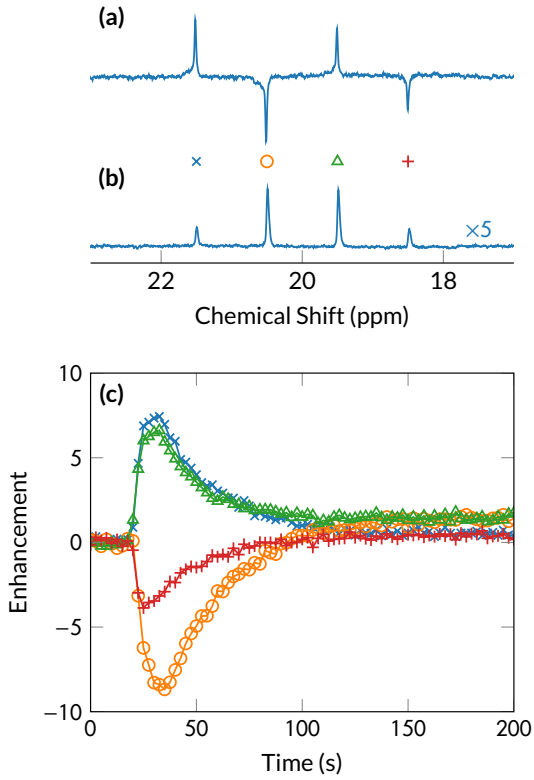

FIGURE 4 D-QRIP Experiment on 2-^{13}C-labelled acetate. A spectrum is recorded every 2.5 s. (a) D-QRIP spectrum, recorded approximately 8s after ejection and dissolution of the sample capsule. (b) Thermal equilibrium spectrum (60 transients averaged), magnified by a factor of 5. (c) Enhancements of the four peaks of the methyl spectrum as a function of time. The enhancement for each signal is calculated as its integral divided by the average integral of the four signals of the thermal equilibrium spectrum.

3.2.2 | Water

Quantum-rotor-induced polarization may also be observed in ^{17}O-labelled, fullerene-encapsulated water. The energy structure of this system is analogous to the one shown in Fig. 2, except that the quantum number of the heteronucleus assumes the values $-5/2, -3/2, \ldots, 5/2$, since ^{17}O has spin $5/2$. The proton spectrum of this substance comprises six peaks due to the J-coupling between the protons and oxygen. Scalar relaxation induced by the quadrupolar relaxation of the ^{17}O nucleus leads to a spectrum that is symmetric, but exhibits different linewidths depending on the ^{17}O spin quantum number [55].

To facilitate rapid dissolution, $H_2^{17}O@C_{60}$ is predissolved in orthodichlorobenzene. This sample is kept at 4.2 Kelvin overnight to enrich the amount of *para*-water. It is then shot into an NMR tube loaded with deuterated toluene. $H_2^{17}O@C_{60}$ exhibits a short ^{1}H T_1 of less than 1 s. Therefore a 30° flip-angle is applied every 250 ms, followed by signal acquisition. Due to the weak enhancements and the low concentration of $H_2^{17}O@C_{60}$ in the final solution the signals are too weak to be observed in a single scan. The spectra obtained from averaging 20 transients in the intervals 5-10 s and 35-40 s after dissolution are shown in Fig. 5a) and b), respectively. A clear antiphase pattern is obtained shortly after

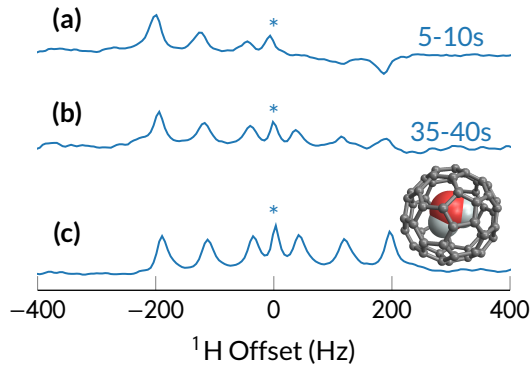

FIGURE 5 D-QRIP Experiment on $H_2^{17}O@C_{60}$. (a) Average of 20 transients recorded in the interval 5-10 s after dissolution of the material. The flip angle of the RF pulse is 30 degrees, one transient is recorded every 250 ms. The spectrum of $H_2^{17}O@C_{60}$ exhibits 6 peaks due to the J-coupling to the spin-5/2 ^{17}O nucleus. The peak at zero offset (*) is due to residual $H_2^{16}O@C_{60}$. The spectrum exhibits an antiphase pattern characteristic of quantum-rotor-induced polarization. (b) The same as (a), but recorded 30 s later, i.e. in the interval 30-35 s. The spin system clearly has not reached thermal equilibrium. (c) Thermal equilibrium spectrum recorded after full equilibration (64 transients averaged). The vertical scale is consistent across (a)-(c).

dissolution. Half a minute later, cross-relaxation is still continuing, and the spectrum is still not symmetric. The thermal equilibrium spectrum, recorded after full equilibration is shown in Fig. 5c). While quantum-rotor-induced polarization is clearly observed, the transient signals happen to be of the same strength as the thermal equilibrium polarization, the enhancement is approximately 1. In part this is anticipated as more long-lived symmetry order implies weaker cross-relaxation processes. If in addition T_1 is short, the polarization is only accumulated for short time, and only small enhancements are obtained. A more detailed analysis of this experiment is available elsewhere [54].

4 | CONCLUDING REMARKS

To date dissolution quantum-rotor-induced polarization has been observed on various methyl moieties as well as on $H_2^{17}O@C_{60}$. The scope of D-QRIP will likely remain limited as only very few substances exhibit sufficiently freely rotating groups. Further progress in the synthesis of molecular endofullerenes will enable the study of new quantum rotors such as $CH_4@C_{60}$, but slow conversion of symmetry order into observable magnetization will limit the attainable enhancements to values that are small compared to what can be achieved with dissolution dynamic nuclear polarization. A way to generate larger enhancements then is to "slow down" or halt the rotor, for example by means of a chemical reaction.

Quantum-rotor-induced polarization is generated as symmetry order is converted into magnetization, and therefore occurs only in molecules that support a long-lived spin state. In fact, the first evidence for long-lived spin states in methyl groups was obtained by exploiting quantum-rotor-induced polarization. In the absence of a rotational splitting, long-lived symmetry order can be established in a range of substances using DNP[56, 23, 30]. The long-lived symmetry order in methyl groups can also be established or in fact enhanced using dynamic nuclear polarization in presence of a small tunneling splitting, as has been shown for protonated methyl groups [31]. This interesting observation implies

that DNP can facilitate symmetry conversion and at least indirectly lower the temperature of the rotational reservoir. Conversely relaxation of the rotational reservoir [57] may influence the buildup of spin polarization.

ACKNOWLEDGEMENTS

I thank Shamim Alom and Richard Whitby for providing the $H_2^{17}O@C_{60}$ material. I would like to thank Karel Kouřil, Hana Kouřilová and Timothy Barker for experimental help, and Stuart Elliott and Christian Bengs for discussions. I thank Karel Kouřil and Malcolm Levitt for reading this manuscript prior to publication, as well as for numerous discussions.

CONFLICT OF INTEREST

The author declares no conflict of interests.

REFERENCES

[1] Jan-Henrik Ardenkjaer-Larsen, Gregory S. Boebinger, Arnaud Comment, Simon Duckett, Arthur S. Edison, Frank Engelke, Christian Griesinger, Robert G. Griffin, Christian Hilty, Hidaeki Maeda, Giacomo Parigi, Thomas Prisner, Enrico Ravera, Jan van Bentum, Shimon Vega, Andrew Webb, Claudio Luchinat, Harald Schwalbe, and Lucio Frydman. Facing and overcoming sensitivity challenges in biomolecular nmr spectroscopy. *Angewandte Chemie International Edition*, 54(32):9162–9185, 2015. doi: 10.1002/anie.201410653. URL http://dx.doi.org/10.1002/anie.201410653.

[2] S. J. Nelson, J. Kurhanewicz, D. B. Vigneron, P. E. Z. Larson, A. L. Harzstark, M. Ferrone, M. van Criekinge, J. W. Chang, R. Bok, I. Park, G. Reed, L. Carvajal, E. J. Small, P. Munster, V. K. Weinberg, J. H. Ardenkjaer-Larsen, A. P. Chen, R. E. Hurd, L.-I. Odegardstuen, F. J. Robb, J. Tropp, and J. A. Murray. Metabolic imaging of patients with prostate cancer using hyperpolarized [1-13c]pyruvate. *Science Translational Medicine*, 5(198):198ra108–198ra108, 2013. doi: 10.1126/scitranslmed.3006070. URL http://dx.doi.org/10.1126/scitranslmed.3006070.

[3] R. W. Adams, J. A. Aguilar, K. D. Atkinson, M. J. Cowley, P. I. P. Elliott, S. B. Duckett, G. G. R. Green, I. G. Khazal, J. Lopez-Serrano, and D. C. Williamson. Reversible interactions with para-hydrogen enhance nmr sensitivity by polarization transfer. *Science*, 323(5922):1708–1711, 2009. doi: 10.1126/science.1168877. URL https://doi.org/10.1126/science.1168877.

[4] J. Hore and R.W. Broadhurst. Photo-cidnp of biopolymers. *Progress in Nuclear Magnetic Resonance Spectroscopy*, 25(4):345–402, 1993. doi: 10.1016/0079-6565(93)80002-b. URL https://doi.org/10.1016/0079-6565(93)80002-b.

[5] Dieter Suter and Fedor Jelezko. Single-spin magnetic resonance in the nitrogen-vacancy center of diamond. *Progress in Nuclear Magnetic Resonance Spectroscopy*, 98-99(nil):50–62, 2017. doi: 10.1016/j.pnmrs.2016.12.001. URL https://doi.org/10.1016/j.pnmrs.2016.12.001.

[6] Patrick Berthault, Gaspard Huber, and Hervé Desvaux. Biosensing using laser-polarized xenon nmr/mri. *Progress in Nuclear Magnetic Resonance Spectroscopy*, 55(1):35–60, 2009. doi: 10.1016/j.pnmrs.2008.11.003. URL https://doi.org/10.1016/j.pnmrs.2008.11.003.

[7] Matthew L. Hirsch, Neal Kalechofsky, Avrum Belzer, Melanie Rosay, and James G. Kempf. Brute-force hyperpolarization for nmr and mri. *Journal of the American Chemical Society*, 137(26):8428–8434, 2015. doi: 10.1021/jacs.5b01252. URL http://dx.doi.org/10.1021/jacs.5b01252.

[8] David T. Peat, Matthew L. Hirsch, David G. Gadian, Anthony J. Horsewill, John R. Owers-Bradley, and James G. Kempf. Correction: Low-field thermal mixing in [1-13c] pyruvic acid for brute-force hyperpolarization. *Phys. Chem. Chem. Phys.*, 18(36):25764–25764, 2016. doi: 10.1039/c6cp90225a. URL http://dx.doi.org/10.1039/c6cp90225a.

[9] Albert W. Overhauser. Polarization of nuclei in metals. *Phys. Rev.*, 92(2):411–415, Oct 1953. ISSN 0031-899X. doi: 10.1103/physrev.92.411. URL http://dx.doi.org/10.1103/physrev.92.411.

[10] T. R. Carver and C. P. Slichter. Polarization of nuclear spins in metals. *Physical Review*, 92(1):212–213, 1953. doi: 10.1103/physrev.92.212.2. URL https://doi.org/10.1103/physrev.92.212.2.

[11] Charles P. Slichter. The discovery and demonstration of dynamic nuclear polarization-a personal and historical account. *Physical Chemistry Chemical Physics*, 12(22):5741, 2010. doi: 10.1039/c003286g. URL https://doi.org/10.1039/c003286g.

[12] Lino R. Becerra, Gary J. Gerfen, Richard J. Temkin, David J. Singel, and Robert G. Griffin. Dynamic nuclear polarization with a cyclotron resonance maser at 5 t. *Physical Review Letters*, 71(21):3561–3564, 1993. doi: 10.1103/physrevlett.71.3561. URL https://doi.org/10.1103/physrevlett.71.3561.

[13] G. J. Gerfen, L. R. Becerra, D. A. Hall, R. G. Griffin, R. J. Temkin, and D. J. Singel. High frequency (140 ghz) dynamic nuclear polarization: Polarization transfer to a solute in frozen aqueous solution. *The Journal of Chemical Physics*, 102(24):9494–9497, 1995. doi: 10.1063/1.468818. URL https://doi.org/10.1063/1.468818.

[14] Edward P. Saliba, Erika L. Sesti, Faith J. Scott, Brice J. Albert, Eric J. Choi, Nicholas Alaniva, Chukun Gao, and Alexander B. Barnes. Electron decoupling with dynamic nuclear polarization in rotating solids. *Journal of the American Chemical Society*, 139(18):6310–6313, 2017. doi: 10.1021/jacs.7b02714. URL http://dx.doi.org/10.1021/jacs.7b02714.

[15] Aany Sofia Lilly Thankamony, Johannes J. Wittmann, Monu Kaushik, and Björn Corzilius. Dynamic nuclear polarization for sensitivity enhancement in modern solid-state nmr. *Progress in Nuclear Magnetic Resonance Spectroscopy*, 102-103(nil):120–195, 2017. doi: 10.1016/j.pnmrs.2017.06.002. URL https://doi.org/10.1016/j.pnmrs.2017.06.002.

[16] J. H. Ardenkjaer-Larsen, B. Fridlund, A. Gram, G. Hansson, L. Hansson, M. H. Lerche, R. Servin, M. Thaning, and K. Golman. Increase in signal-to-noise ratio of >10,000 times in liquid-state NMR. *Proceedings of the National Academy of Sciences*, 100(18):10158–10163, 2003. doi: 10.1073/pnas.1733835100. URL http://dx.doi.org/10.1073/pnas.1733835100.

[17] Xiao Ji, Aurélien Bornet, Basile Vuichoud, Jonas Milani, David Gajan, Aaron J. Rossini, Lyndon Emsley, Geoffrey Bodenhausen, and Sami Jannin. Transportable hyperpolarized metabolites. *Nature Communications*, 8(nil):13975, 2017. doi: 10.1038/ncomms13975. URL http://dx.doi.org/10.1038/ncomms13975.

[18] Aurélien Bornet, Arthur Pinon, Aditya Jhajharia, Mathieu Baudin, Xiao Ji, Lyndon Emsley, Geoffrey Bodenhausen, Jan Henrik Ardenkjaer-Larsen, and Sami Jannin. Microwave-gated dynamic nuclear polarization. *Phys. Chem. Chem. Phys.*, 18(44):30530–30535, 2016. doi: 10.1039/c6cp05587g. URL http://dx.doi.org/10.1039/c6cp05587g.

[19] Greg Olsen, Evgeny Markhasin, Or Szekely, Christian Bretschneider, and Lucio Frydman. Optimizing water hyperpolarization and dissolution for sensitivity-enhanced 2d biomolecular nmr. *Journal of Magnetic Resonance*, 264(nil):49–58, 2016. doi: 10.1016/j.jmr.2016.01.005. URL http://dx.doi.org/10.1016/j.jmr.2016.01.005.

[20] C. Russell Bowers and D. P. Weitekamp. Parahydrogen and synthesis allow dramatically enhanced nuclear alignment. *Journal of the American Chemical Society*, 109(18):5541–5542, 1987. doi: 10.1021/ja00252a049. URL https://doi.org/10.1021/ja00252a049.

[21] Richard A. Green, Ralph W. Adams, Simon B. Duckett, Ryan E. Mewis, David C. Williamson, and Gary G.R. Green. The theory and practice of hyperpolarization in magnetic resonance using parahydrogen. *Progress in Nuclear Magnetic Resonance Spectroscopy*, 67(nil):1–48, 2012. doi: 10.1016/j.pnmrs.2012.03.001. URL http://dx.doi.org/10.1016/j.pnmrs.2012.03.001.

[22] Malcolm H. Levitt. Singlet nuclear magnetic resonance. *Annu. Rev. Phys. Chem.*, 63(1):89–105, May 2012. ISSN 1545-1593. doi: 10.1146/annurev-physchem-032511-143724. URL http://dx.doi.org/10.1146/annurev-physchem-032511-143724.

[23] Daniele Mammoli, Basile Vuichoud, Aurélien Bornet, Jonas Milani, Jean-Nicolas Dumez, Sami Jannin, and Geoffrey Bodenhausen. Hyperpolarized para-ethanol. *The Journal of Physical Chemistry B*, 119(10):4048–4052, 2015. doi: 10.1021/jp512128c. URL http://dx.doi.org/10.1021/jp512128c.

[24] Razieh Annabestani and David G. Cory. Dipolar relaxation mechanism of long-lived states of methyl groups. *Quantum Information Processing*, 17(1):15, 2017. doi: 10.1007/s11128-017-1777-6. URL https://doi.org/10.1007/s11128-017-1777-6.

[25] A.J. Horsewill. Quantum tunnelling aspects of methyl group rotation studied by nmr. *Progress in Nuclear Magnetic Resonance Spectroscopy*, 35(4):359–389, Dec 1999. ISSN 0079-6565. doi: 10.1016/s0079-6565(99)00016-3. URL http://dx.doi.org/10.1016/s0079-6565(99)00016-3.

[26] Maik Icker and Stefan Berger. Unexpected multiplet patterns induced by the haupt-effect. *Journal of Magnetic Resonance*, 219:1–3, Jun 2012. ISSN 1090-7807. doi: 10.1016/j.jmr.2012.03.021. URL http://dx.doi.org/10.1016/j.jmr.2012.03.021.

[27] Maik Icker, Pascal Fricke, and Stefan Berger. Transfer of the haupt-hyperpolarization to neighbor spins. *Journal of Magnetic Resonance*, 223:148–150, Oct 2012. ISSN 1090-7807. doi: 10.1016/j.jmr.2012.07.019. URL http://dx.doi.org/10.1016/j.jmr.2012.07.019.

[28] Benno Meier, Jean-Nicolas Dumez, Gabriele Stevanato, Joseph T. Hill-Cousins, Soumya Singha Roy, Pär Håkansson, Salvatore Mamone, Richard C. D. Brown, Giuseppe Pileio, and Malcolm H. Levitt. Long-lived nuclear spin states in methyl groups and quantum-rotor-induced polarization. *J. Am. Chem. Soc.*, 135(50):18746–18749, 2013. doi: 10.1021/ja410432f. URL http://dx.doi.org/10.1021/ja410432f.

[29] Jean-Nicolas Dumez, Pär Håkansson, Salvatore Mamone, Benno Meier, Gabriele Stevanato, Joseph T. Hill-Cousins, Soumya Singha Roy, Richard C. D. Brown, Giuseppe Pileio, and Malcolm H. Levitt. Theory of long-lived nuclear spin states in methyl groups and quantum-rotor induced polarisation. *The Journal of Chemical Physics*, 142(4):044506, 2015. doi: 10.1063/1.4906273. URL http://dx.doi.org/10.1063/1.4906273.

[30] Aditya Jhajharia, Emmanuelle M. M. Weber, James G. Kempf, Daniel Abergel, Geoffrey Bodenhausen, and Dennis Kurzbach. Communication: Dissolution dnp reveals a long-lived deuterium spin state imbalance in methyl groups. *The Journal of Chemical Physics*, 146(4):041101, 2017. doi: 10.1063/1.4974358. URL http://dx.doi.org/10.1063/1.4974358.

[31] Jean-Nicolas Dumez, Basile Vuichoud, Daniele Mammoli, Aurélien Bornet, Arthur C. Pinon, Gabriele Stevanato, Benno Meier, Geoffrey Bodenhausen, Sami Jannin, and Malcolm H. Levitt. Dynamic nuclear polarization of long-lived nuclear spin states in methyl groups. *The Journal of Physical Chemistry Letters*, 8(15):3549–3555, 2017. doi: 10.1021/acs.jpclett.7b01512. URL https://doi.org/10.1021/acs.jpclett.7b01512.

[32] Jack H. Freed. Quantum effects of methyl-group rotations in magnetic resonance: Esr splittings and linewidths. *The Journal of Chemical Physics*, 43(5):1710–1720, 1965. doi: 10.1063/1.1696995. URL https://doi.org/10.1063/1.1696995.

[33] Roberto Buratto, Daniele Mammoli, Estel Canet, and Geoffrey Bodenhausen. Ligand-protein affinity studies using long-lived states of fluorine-19 nuclei. *Journal of Medicinal Chemistry*, 59(5):1960–1966, 2016. doi: 10.1021/acs.jmedchem.5b01583. URL http://dx.doi.org/10.1021/acs.jmedchem.5b01583.

[34] C. Ludwig, M. Saunders, I. Marin-Montesinos, and U. L. Gunther. Quantum rotor induced hyperpolarization. *Proceedings of the National Academy of Sciences*, 107(24):10799–10803, May 2010. ISSN 1091-6490. doi: 10.1073/pnas.0908421107. URL http://dx.doi.org/10.1073/pnas.0908421107.

[35] Maik Icker, Pascal Fricke, Toni Grell, Julia Hollenbach, Henry Auer, and Stefan Berger. Experimental boundaries of the quantum rotor induced polarization (qrip) in liquid state nmr. *Magnetic Resonance in Chemistry*, 51(12):815–820, Oct 2013. ISSN 0749-1581. doi: 10.1002/mrc.4021. URL http://dx.doi.org/10.1002/mrc.4021.

[36] Somayeh Khazaei and Daniel Sebastiani. Tunneling of coupled methyl quantum rotors in 4-methylpyridine: Single rotor potential versus coupling interaction. *The Journal of Chemical Physics*, 147(19):194303, 2017. doi: 10.1063/1.5003081. URL https://doi.org/10.1063/1.5003081.

[37] Claude Cohen-Tannoudji, Bernard Diu, and Franck Laloe. *Quantum Mechanics*. John Wiley, 2005. ISBN 978-0-471-56952-7. URL https://books.google.co.uk/books?id=crewAgvSUAMC.

[38] Javier Alonso-Valdesueiro, Stuart J. Elliott, Christian Bengs, Benno Meier, and Malcolm H. Levitt. Testing signal enhancement mechanisms in the dissolution nmr of acetone. *Journal of Magnetic Resonance*, 286(nil):158–162, 2018. doi: 10.1016/j.jmr.2017.12.009. URL https://doi.org/10.1016/j.jmr.2017.12.009.

[39] Philip R. Bunker and Per Jensen. *Molecular Symmetry and Spectroscopy*. National Research Council of Canada, 2006. ISBN 0-660-19628-X.

[40] M. Prager and A. Heidemann. Rotational tunneling and neutron spectroscopy: A compilation. *Chemical Reviews*, 97(8): 2933–2966, 1997. doi: 10.1021/cr9500848. URL http://dx.doi.org/10.1021/cr9500848.

[41] François Fillaux, Béatrice Nicolaï, Werner Paulus, Erika Kaiser-Morris, and Alain Cousson. Collective rotational tunneling of methyl groups and quantum solitons in 4-methylpyridine: Neutron scattering studies of single crystals. *Physical Review B*, 68(22), Dec 2003. ISSN 1095-3795. doi: 10.1103/physrevb.68.224301. URL http://dx.doi.org/10.1103/physrevb.68.224301.

[42] C. Beduz, M. Carravetta, J. Y.-C. Chen, M. Concistre, M. Denning, M. Frunzi, A. J. Horsewill, O. G. Johannessen, R. Lawler, X. Lei, and et al. Quantum rotation of ortho and para-water encapsulated in a fullerene cage. *Proceedings of the National Academy of Sciences*, 109(32):12894–12898, Jul 2012. ISSN 1091-6490. doi: 10.1073/pnas.1210790109. URL http://dx.doi.org/10.1073/pnas.1210790109.

[43] J. Haupt. A new effect of dynamic polarization in a solid obtained by rapid change of temperature. *Physics Letters A*, 38 (6):389–390, Mar 1972. ISSN 0375-9601. doi: 10.1016/0375-9601(72)90219-8. URL http://dx.doi.org/10.1016/0375-9601(72)90219-8.

[44] J. Haupt. Experimental results on the dynamic nuclear polarisation in a solid by variation of temperature. *Z. Naturforsch.*, 28a(nil):98–104, December 1972. ISSN 0375-9601. doi: 10.1016/0375-9601(72)90219-8. URL nil.

[45] M. Tomaselli, C. Degen, and B. H. Meier. Haupt magnetic double resonance. *The Journal of Chemical Physics*, 118(19): 8559–8562, 2003. doi: 10.1063/1.1573635. URL http://scitation.aip.org/content/aip/journal/jcp/118/19/10.1063/1.1573635.

[46] M. Tomaselli, U. Meier, and B. H. Meier. Tunneling-induced spin alignment at low and zero field. *The Journal of Chemical Physics*, 120(9):4051–4054, 2004. doi: 10.1063/1.1649315. URL https://doi.org/10.1063/1.1649315.

[47] Richard L. Redington and Dolphus E. Milligan. Molecular rotation and ortho-para nuclear spin conversion of water suspended in solid ar, kr, and xe. *The Journal of Chemical Physics*, 39(5):1276–1284, 1963. doi: 10.1063/1.1734427. URL http://dx.doi.org/10.1063/1.1734427.

[48] Russell Sliter, Melissa Gish, and Andrey F. Vilesov. Fast nuclear spin conversion in water clusters and ices: A matrix isolation study. *The Journal of Physical Chemistry A*, 115(34):9682–9688, 2011. doi: 10.1021/jp201125k. URL http://dx.doi.org/10.1021/jp201125k.

[49] K. Kurotobi and Y. Murata. A single molecule of water encapsulated in fullerene c60. *Science*, 333(6042):613–616, 2011. doi: 10.1126/science.1206376. URL https://doi.org/10.1126/science.1206376.

[50] Andrea Krachmalnicoff, Malcolm H. Levitt, and Richard J. Whitby. An optimised scalable synthesis of h2o@c60 and a new synthesis of h2@c60. *Chem. Commun.*, 50(86):13037–13040, 2014. doi: 10.1039/c4cc06198e. URL https://doi.org/10.1039/c4cc06198e.

[51] Salvatore Mamone, Maria Concistrè, Elisa Carignani, Benno Meier, Andrea Krachmalnicoff, Ole G. Johannessen, Xuegong Lei, Yongjun Li, Mark Denning, Marina Carravetta, Kelvin Goh, Anthony J. Horsewill, Richard J. Whitby, and Malcolm H. Levitt. Nuclear spin conversion of water inside fullerene cages detected by low-temperature nuclear magnetic resonance. *The Journal of Chemical Physics*, 140(19):194306, 2014. doi: 10.1063/1.4873343. URL http://dx.doi.org/10.1063/1.4873343.

[52] Daniel A. Horke, Yuan-Pin Chang, Karol Długołęcki, and Jochen Küpper. Separating para and ortho water. *Angewandte Chemie International Edition*, 53(44):11965–11968, 2014. doi: 10.1002/anie.201405986. URL https://doi.org/10.1002/anie.201405986.

[53] Benno Meier, Salvatore Mamone, Maria Concistrè, Javier Alonso-Valdesueiro, Andrea Krachmalnicoff, Richard J. Whitby, and Malcolm H. Levitt. Electrical detection of ortho-para conversion in fullerene-encapsulated water. *Nature Communications*, 6(nil):8112, 2015. doi: 10.1038/ncomms9112. URL http://dx.doi.org/10.1038/ncomms9112.

[54] B. Meier, K. Kouřil, C. Bengs, H. Kouřilová, T. J. Barker, S. J. Elliott, S. Alom, R. J. Whitby, and M. H. Levitt. Spin-isomer conversion of water at room temperature, and quantum-rotor-induced nuclear polarization, in the water-endofullerene H_2O@C_60. *ArXiv e-prints*, February 2018.

[55] Stuart J. Elliott, Christian Bengs, Karel Kouril, Benno Meier, Shamim Alom, Richard J. Whitby, and Malcolm Harris Levitt. Nmr lineshapes and scalar relaxation of the 17o-labelled water-endofullerene h2o@c60. *ChemPhysChem*, nil(nil):nil, 2017. doi: 10.1002/cphc.201701330. URL https://doi.org/10.1002/cphc.201701330.

[56] Michael C. D. Tayler, Irene Marco-Rius, Mikko I. Kettunen, Kevin M. Brindle, Malcolm H. Levitt, and Giuseppe Pileio. Direct enhancement of nuclear singlet order by dynamic nuclear polarization. *J. Am. Chem. Soc.*, 134(18):7668–7671, 2012. doi: 10.1021/ja302814e. URL http://dx.doi.org/10.1021/ja302814e.

[57] S Clough, A J Horsewill, and M N J Paley. Dynamic nuclear polarisation by the cooling of tunnelling methyl groups. *Journal of Physics C: Solid State Physics*, 15(17):3803–3808, 1982. doi: 10.1088/0022-3719/15/17/018. URL http://dx.doi.org/10.1088/0022-3719/15/17/018.

APPENDIX

Less than twenty lines of Python code are required to compute the energies of the 1D methyl rotor, using Python's Numpy library. A full listing, written using the freely available IPython Notebook, is given below. Note the computation has been performed in wavenumbers, which are easier to handle computationally. To convert to wavenumbers, the matrix elements as given in the manuscript are multiplied by $1/\hbar c$.

```
import numpy as np
import matplotlib.pyplot as plt
%matplotlib inline

from scipy.constants import c, hbar, e

def wavenumbersToEV(x):
    return np.array(x)*hbar*c/e

I = 5.31e-47
V3 = 1e-3*e #one meV

# Setup Hamiltonian, energies in wavenumbers
# The free rotor Hamiltonian in the free rotor
# basis has entries only on the diagonal.
# The code below creates the corresponding diagonal matrix.
maxN = 150
freeRotor = np.diag([hbar*n**2/(c*2*I)
                     for n in range(-maxN/2+1, maxN/2+1)])

# The potential term for the three-fold potential leads to entries
# on the main diagonal (first line),
# and on the off-diagonals shifted by +/- 3 (second/third line).
potential3 = (2*np.identity(maxN)
              - np.diag(np.ones(maxN - 3), 3)
              - np.diag(np.ones(maxN - 3), -3))

potentialTerm = V3/(4*hbar*c)*potential3

# Calculate eigenvalues for no potential, 10 meV, and 100 meV.
for scaleFactor in [0,10,100]:
    # The Hamiltonian H is the sum of the free rotor Hamiltonian
    # and the potential .
    H = freeRotor + scaleFactor*potentialTerm

    # np.linalg.eig returns the eigenvalues or energies,
    # and the eigenvectors, or eigenstates.
    energies, basisFunctions = np.linalg.eig(H)

    # Now plot a sorted list of the energies to
    # reveal the energy structure.
    plt.plot(wavenumbersToEV(sorted(energies)), "-x",
             label = "V3 = {} meV".format(scaleFactor))
```

GRAPHICAL ABSTRACT

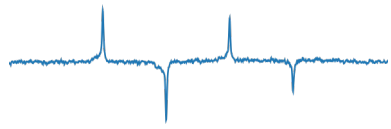

Quantum-rotor-induced polarization is closely related to para-hydrogen-induced polarization. In both cases hyperpolarized spin order derives from rotational interaction, and the Pauli principle by which the symmetry of the spin state dictates the symmetry of the rotational state. This review discusses preconditions for quantum-rotor-induced polarization in the 1-dimensional methyl rotor and in the asymmetric rotor $H_2^{17}O@C_{60}$, i.e. a single water molecule encapsulated in fullerene C_{60}. Experimental results are presented for both rotors.